Phys Chem Minerals (1988) 15:398–408

PHYSICS AND CHEMISTRY OF MINERALS
© Springer-Verlag 1988

5248

Orbital Interactions in Phyllosilicates: Perturbations of an Idealized Two-dimensional, Infinite Silicate Frame

William F. Bleam[1] and Roald Hoffmann[2]

[1] Eastern Regional Research Center, USDA-ARS, 600 E. Mermaid Lane, Philadelphia, PA 19118, USA
[2] Department of Chemistry and Materials Science Center, Cornell University, Ithaca, NY 14853, USA

Abstract. The $^2_\infty[Si_2O_5^{2-}]$ frame in phyllosilicate minerals is distorted through the rotation and tilting of the silicate tetrahedra and interacts with octahedral cations through its apical oxygens. Qualitative perturbation theory and extended Hückel band structure calculations demonstrate that rotation and tilting distortions of the $^2_\infty[Si_2O_5^{2-}]$ frame have little influence on orbital interactions within the frame. The effects which are observed can be traced to next-nearest-neighbor, oxygen-oxygen interactions. Analysis of band widths and crystal-orbital-overlap-populations demonstrate the importance of O(2*s*) orbitals in the silicate bond. Interactions between Si(3*s*, 3*p*) and O(2*s*) atomic orbitals account for about half of the bonding overlap in the Si-O bond. Crystal orbitals within the $^2_\infty[Si_2O_5^{2-}]$ frame are perturbed in kaolinite, lizardite, pyrophyllite and talc through interactions of the apical oxygens with octahedrally coordinated Al(III) and Mg(II). These interactions appear to involve states that are non-bonding in an isolated frame, having little effect on the Si-O_{apical} bond while significantly reducing the apical-oxygen atomic population.

Introduction

All phyllosilicates have structures based on two-dimensional silicate sheets. In this paper we attempt to lay the foundation for a conceptual understanding of isomorphous substitution in phyllosilicates by examining the structure and bonding of neutral-layer minerals which exemplify the basic structural motifs of the class as a whole.

The minerals we have chosen to examine in this paper are: kaolinite, lizardite, pyrophyllite and talc. The Al(III) and Mg(II) in kaolinite $[Al_2(OH)_4Si_2O_5]$ and lizardite $[Mg_3(OH)_4Si_2O_5]$ reside in six-fold coordination sites located between a plane of hydroxyl ions and a single silicate sheet (Fig. 1a). Al(III) ions occupy two-thirds of the total available six-fold coordination sites in kaolinite layers, refered to as the octahedral sheet, while Mg(II) ions populate every available six-fold coordination site in lizardite. The six-fold coordination sites are found between two silicate sheets in pyrophyllite $[Al_2(OH)_2(Si_2O_5)_2]$ and talc $[Mg_3(OH)_2(Si_2O_5)_2]$ (Fig. 1b). We can readily derive nearly all phyllosilicate structures through substitutions in the four listed above.

The two-dimensional, infinite $[Si_2O_5^{2-}]$-tetrahedral-sheet will be our point of departure. Our approach will be to conceptually build the minerals we are studying from the following components: $^2_\infty[Si_2O_5^{2-}]$-sheets, the cations Mg(II) or Al(III), and hyroxyl ions. In constructing these phyllosilicates we will first examine the orbital interactions within the framework and how they are influenced by distortion. We will complete our study by looking at the interactions of the silicate framework with Mg(II) and Al(III) in actual minerals.

We wish to develop a physical understanding of orbital interactions in phyllosilicates. Our calculations were done using the extended Hückel, tight-binding method (Hoffmann 1963, Hoffmann and Lipscomb 1962, Whangbo et al. 1979). The parameters and other details relating to the calculations are found in the Appendix.

Bonding in Phyllosilicates

Silicates have rather "open" structures with 2-fold and 4-fold coordinated atoms, a classic indication of structures where orbital interactions (which give rise to directional bonds) are important in the bonding (Pantelides and Harrison 1976). Although the $^2_\infty[Si_2O_5^{2-}]$-frame of phyllosilicates is an "open" structure, involving orbital interactions within and between silicate tetrahedra sufficient to overcome the tendency toward close packing, the bonding is highly polar (Harrison 1980).

In a solid with pure ionic bonding the occupied states, constituting the valence bands, can be completely con-

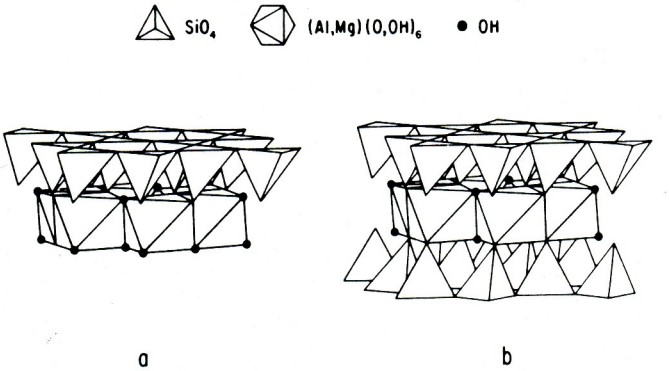

Fig. 1a, b. Phyllosilicate crystal structures, (**a**) $[Al_2(OH)_4Si_2O_5]$ or $[Mg_3(OH)_4Si_2O_5]$ and (**b**) $[Al_2(OH)_2(Si_2O_5)_2]$ or $[Mg_3(OH)_2(Si_2O_5)_2]$

structed from anion orbitals while the unoccupied states, constituting the conducting bands, can be derived entirely from cation orbitals. Orbital interactions in silicates "mix" some silicon character into the valence bands and some oxygen character into the conducting bands, yet the bonding is sufficiently polar that the valence bands can be essentially thought of as perturbed oxygen states.

Bennett and Roth (1971), in an early study of orbital interactions in silicon dioxide, limited their analysis to "O(2*p*)" states. They found the lowest valence states involved significant Si(3*s*)−O(2*p*) mixing, but the highest O(2*p*) states contained little silicon character. Breeze and Perkins (1973) reported the first band structure and *density-of-states* (DOS) calculations on silicon dioxide using a slightly modified form of extended Hückel theory. They attribute the lower part of the "O(2*p*)" bands to Si(3*s*)−O(2*p*) interactions, the middle to Si(3*p*)−O(2*p*) interactions, and describe the uppermost as non-bonded O(2*p*) states. Their results also show that bands involving Si(3*s*) character have the greatest dispersion, i.e. cover the greatest energy range. In fact, the dispersion of the "O(2*s*)" bands in nearly the same as the "O(2*p*)" bands. The greater the dispersion or width of a band, the larger the orbital interaction.

Breeze and Perkins (1973) made a very important observation. In the regions where Si(3*s*)−O(2*p*) interactions predominate "each wavefunction incorporates only a very small amount of silicon 3*s*. However, the density of states in [this region] is extremely high and hence the *total* amount of silicon 3*s* density is quite high."

To properly assess the importance of a given interaction in solids we must consider both the magnitude of the orbital coefficient in a given state and the total number of states to which this orbital contributes. Atomic orbital coefficients in *linear-combination-of-atomic-orbitals* (LCAO) wavefunctions have led many to assume that O(2*s*) states can be treated as non-bonding, "core" states (Tossell and Gibbs 1977; Brytov et al. 1979; Tossell 1975). Band structure calculations on silicon dioxide conflict with that conclusion (Pantelides and Harrison 1976).

Silicon dioxide polymorphs are the only silicate minerals for which band structure or DOS calculations using the full symmetry of the solid have been reported. There have been two LCAO calculations on phyllosilicate structures, Peterson et al. (1979) and Aronowitz et al. (1982). Both of these studies have used molecular orbital calculations performed on "clusters" chosen to represent certain features of phyllosilicate structures. While they do not examine orbital interactions explicitly, their results are broadly consistent with previously cited studies of SiO_2.

Idealized Phyllosilicate Structures

The only restriction on the symmetry of the $^2_\infty[Si_2O_5^{2-}]$, tetrahedral sheet incorporated into a phyllosilicate layer is that it must share symmetry elements with the octahedral sheet; i.e., contain them as a subgroup. In this study we have "idealized" all of the structures by using perfect tetrahedra and trigonal anti-prisms and by restricting all bond lengths of a given type; d(Si−O), d(Al−O), d(Mg−O) or d(O−H); to be the same.

Longer bonds are found at those contacts with less than average overlap population while shorter bonds are associated with contacts having greater than average overlap population (Gibbs et al. 1972; Louisnathan and Gibbs 1972a; Louisnathan and Gibbs 1972b). Comparison of overlap populations can only be made for the same type of bond; i.e., n(Si−O) cannot be compared to n(Al−O) since their orbital exponents put them on different scales. Furthermore, the comparison is fair only when all bonds to be compared are at equal length in the calculation. Otherwise, the normal tendency of greater overlap population to be associated with shorter bond lengths will prejudice the calculations.

We found that tetrahedral tilting, which produces "corrugations" in kaolinite and pyrophyllite, has a negligible effect on the electronic structure and therefore chose to further idealize the kaolinite and pyrophyllite structures in our calculations by eliminating this distortion. In these two minerals we use a $^2_\infty[Si_2O_5^{2-}]$, tetrahedral sheet with symmetry *p31m* (Fig. 2b, see Vainshtein (1981) for a discussion of layer groups), produced by 10° alternating left- and right-hand tetrahedral rotations around the six-fold rings (Suitch and Young 1983; Zvyangin 1960), and have all Al in the "gibbsite" sheet co-planar in trigonal anti-prisms. The bond lengths, sub-unit symmetries and other details for our structures appear in the Appendix.

Perturbation Theory of Orbital Interactions in the Isolated $^2_\infty[Si_2O_5^{2-}]$ *p6mm* Framework

There is a symmetry element, namely a mirror plane, common to layer groups *p6mm*, *p31m*, *c2/m* and *c1m1* (Vainshtein 1981). Later we will compare the energies of electronic states for reciprocal-space wave vectors, from the center of the first Brillouin zone to its edge, contained in this common mirror plane. For now we will be interested in a simple analysis, cast in the language of perturbation theory (Albright, Burdett and Whangbo 1985), of orbital interactions at the center of the Brillouin zone. States along the symmetry line contained within the mirror plane can be readily derived from the picture at the center of the Brillouin zone (Tinkham 1964).

The fundamental, unifying element of all silicates is the silicate tetrahedron, where four oxygen atoms coordinate a silicon atom. We will begin by grouping the oxygen atoms into symmetry-equivalent sets (cf. Albright, Burdett and Whangbo 1985). Next, the atomic orbitals of each equivalent set are classed according to their transformation properties under the operations of the layer group. Orbital interactions occur between symmetry-adapted combinations of oxygen orbitals and silicon orbitals belonging to the same irreducible representation of the layer group.

Some theorists have considered O(2*s*) orbitals to be non-bonding, "core" states (Harrison 1977; Tossell and Gibbs 1977; Brytov et al. 1979; Tossell 1975). Let us examine this approximation. The *valence orbital ionization potentials* (VOIP) for O(2*s*) and O(2*p*) used in this calculation are −32.3 eV and −14.8 eV, respectively (Summerville and Hoffmann 1976). These compare well with empirical and calculated values (Cusachs and Corrington 1970) where the energy separation between O(2*s*) and O(2*p*) orbital energies fall in the range of 15.0 to 17.5 eV. XES, XPS and UPS spectra from silicates (DiStefano and Eastman 1971; Tossell et al. 1973; Schneider and Fowler 1976; Schlüter and Chelikowsky 1977; Dikov et al. 1977; Pantelides 1977) indicate the separation between non-bonded, O(2*p*) states and states derived from O(2*s*) orbitals is some 20 eV. While

Table 1. First Brillouin zone symmetry points and lines

Layer group	$\mathbf{k}_\Gamma$	$\mathbf{k}_K$	$\mathbf{k}_M$	$\mathbf{k}_{\Lambda(\Gamma K)}$	$\mathbf{k}_{\Sigma(\Gamma M)}$	$\mathbf{k}_{T(MK)}$
p6mm	*6mm*	*3m*	*2mm*	*m*	*m*	*m*
p31m	*3m*	*3*	*m*	*m*	*1*	*1*
c1m1	*m*	*m*	*1*	*m*	*1*	*1*
c2/m	*2/m*	*m*	*1*	*m*	*1*	*1*

Reciprocal-space basis vectors: $\mathbf{g}_1=(2\pi/a\sqrt{3}, -2\pi/a)$ and $\mathbf{g}_2=(4\pi/a\sqrt{3}, 0)$. $\mathbf{k}_\Gamma=[0,0]$; $\mathbf{k}_K=[2/3,1/3]$; $\mathbf{k}_M=[1/2,0]$; $\mathbf{k}_{\Lambda(\Gamma K)}=[2\alpha, \alpha], 0<\alpha<1/3$; $\mathbf{k}_{\Sigma(\Gamma M)}=[\beta, 0]$, $0<\beta<1/2$; $\mathbf{k}_{T(MK)}=[1/2+\gamma, 2\gamma]$, $0<\gamma<1/6$

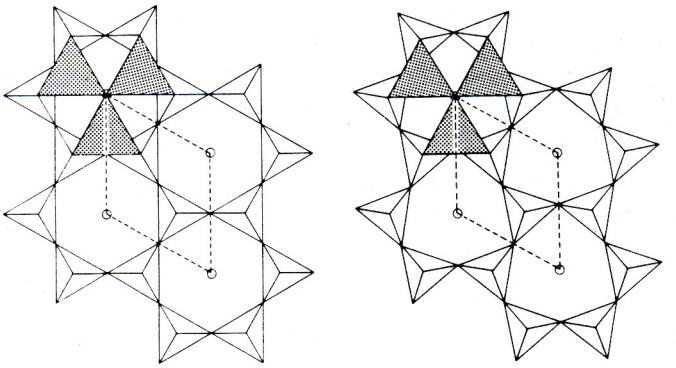

a b

Fig. 2a, b. Tetrahedral sheets showing the primative cell and bases of the trigonal antiprisms (shaded) above which lie the "octahedral" cation sites: **(a)** *p6mm*, $^2_\infty[Si_2O_5^{2-}]$ and **(b)** *p31m*, $^2_\infty[Si_2O_5^{2-}]$

next-nearest-neighbor interactions will broaden the non-bonded, O(2*p*) bands, these will be centered near the VIOP of the isolated atomic orbital. Experimental findings *suggest* that O(2*s*) orbitals are stabilized 2.5 to 5 eV by bonding interactions with silicon orbitals in silicates and we will assume O(2*s*) orbitals are involved in orbital interactions in the discussion that follows.

As we indicated above, our discussion will involve only orbital interactions at the center of the Brillouin zone. The relevant layer group will be the layer group of the reciprocal-space wave vector at Γ, $\mathbf{k}_\Gamma$. The point groups isomorphic to the various layer groups of $\mathbf{k}_\Gamma$ in this discussion appear in Table 1. For instance, the point group isomorphic to the layer group of $\mathbf{k}_\Gamma$ for a two-dimensional silicate sheet with layer group symmetry *p6mm* is *6mm* (Fig. 2a). We will use the contents of the primitive cell to illustrate orbital interactions at $\mathbf{k}_\Gamma$. Although our illustrations for the following discussion will show what appears to be $[Si_2O_7^{4-}]$, we are actually dealing with the repeat unit $[Si_2O_5^{2-}]$.

There are five oxygens and two silicons per primitive cell in our $^2_\infty[Si_2O_5^{2-}]$ frames, giving a total of twenty-eight valence orbitals. Since silicates are highly polar solids, to zeroth order in perturbation theory we can treat the valence bands as essentially oxygen states and the conduction bands as silicon states. This means that in the two-dimensional, infinite $^2_\infty[Si_2O_5^{2-}]$-frame we expect to find twenty occupied, valence bands and eight unoccupied, conduction bands derived from oxygen and silicon valence orbitals.

The five O(2*s*) orbitals, grouped according to their irreducible representations in the *p6mm* layer group, appear in Figure 3. There are two a_1 and one each of b_2 and e_2. The linear combinations of oxygen O(2*p*) orbitals transform as five irreducible representations in *p6mm*, forming two a_1, one b_1, two b_2, three e_1 and two e_2 sets of symmetry-adapted combinations. Zeroth-order degeneracy is removed by next-nearest-neighbor, oxygen-oxygen interactions. To first order we would expect combinations belonging to the same irreducible representation to mix. We will assume that to second order "sp-mixing" of oxygen orbitals can be neglected. XES, XPS and UPS studies (DiStefano and Eastman 1971; Tossell et al. 1973; Schneider and Fowler 1976; Schlüter and Chelikowsky 1977; Dikov et al. 1977; Pantelides 1977) support this assumption.

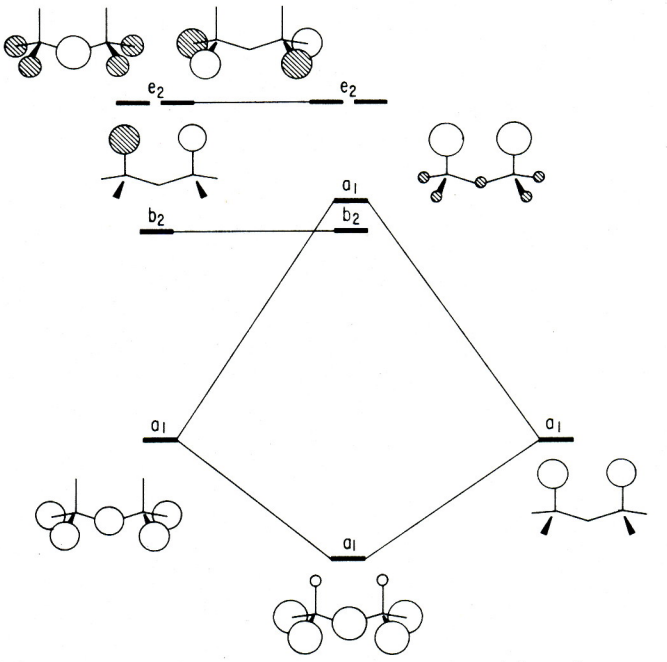

Fig. 3. Interaction diagram showing first-order mixing of symmetry-adapted combinations of O(2*s*) orbitals of an idealized, *p6mm* tetrahedral sheet, $^2_\infty[Si_2O_5^{2-}]$, at the center of the Brillouin zone

The Si(3*s*) and Si(3*p*) orbitals can also be classified by their irreducible representations. One can prepare two a_1 and b_2 combinations from the Si(3*s*) and Si(3*p*) orbitals. We will not go into the details of orbital mixing. Suffice to say that one can prepare linear combinations of the silicon orbitals using the same principles we used for the O(2*s*) orbitals. $SiL_{2,3}$ and $SiK\beta XES$ spectra indicate second-order "sp-mixing" of silicon valence atomic orbitals (Pantelides and Harrison 1976). The final qualitative picture of orbital interactions between Si(3*s*, 3*p*) and O(2*s*) results in the bonding orbitals appearing in Figure 4a–4d.

A similar perturbation analysis can be made for Si(3*s*, 3*p*)−O(2*p*) interactions. O(2*p*) linear combinations transforming as e_1 and b_2 interact with the silicon e_1 and b_2 combinations as seen in Figures 4e and 4f. The remaining O(2*p*) combinations, which are degenerate to zeroth order, have their degeneracies removed to first order through next-nearest-neighbor, oxygen-oxygen interactions. There is only one state that is strictly non-bonding by symmetry, a single b_1 combination of basal oxygens for which there is no counterpart among the combinations of silicon orbitals. The combinations not illustrated in Figure 4 and not transforming as b_1 are treated as non-bonding.

Looking ahead, when we "turn on" interactions between the $^2_\infty[Si_2O_5^{2-}]$ frame and the atoms in the octahedral

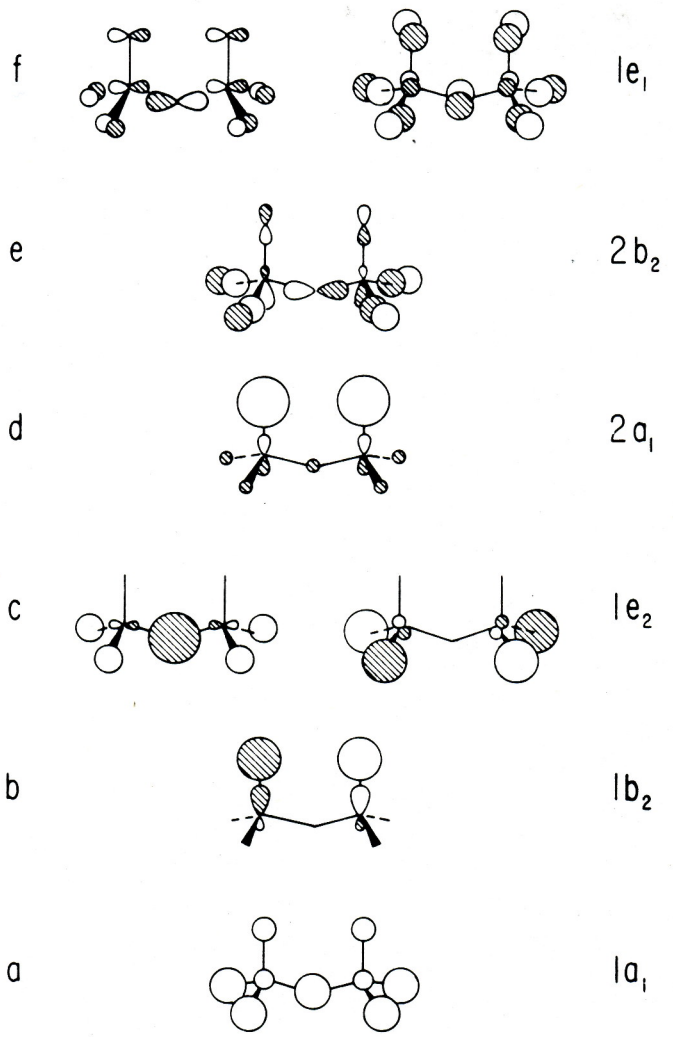

Fig. 4. Bonding orbitals for an idealized, *p6mm* tetrahedral sheet, $^2_\infty[Si_2O_5^{2-}]$, at the center of the Brillouin zone

sheet in kaolinite, lizardite and the other minerals, the picture we have sketched above will change. Some states of the isolated frame will remain essentially unperturbed, the most likely candidates being those like $1e_2$ with no oxygen orbitals in the apical position. States such as $1b_2$ and $2a_1$, where the orbitals on the apical oxygens are prominent, will be most sensitive to perturbing interactions in phyllosilicate minerals.

We have presented a qualitative picture of orbital interactions in the *p6mm*, $^2_\infty[Si_2O_5^{2-}]$ frame using perturbation theory. We have assumed O(2*s*) orbitals are important in Si–O bonding. The essential features of this analysis can be expressed in simple terms. First, there are twenty filled bands that can be grouped into two sets: five "O(2*s*)" bands and fifteen "O(2*p*)" bands. Orbital interactions of symmetry-adapted oxygen combinations with similarly prepared silicon orbitals are treated as perturbations of the "oxygen" bands. Second, after allowing mixing of oxygen combinations transforming as the same irreducible representation and "sp-mixing" on silicon, we formed eight bonding states (two are doubly degenerate) and twelve nonbonding states (four are doubly degenerate). This compares with our expectation of eight Si–O bonds and twelve lone-pair orbitals (two each on the basal, bridging oxygens and three each on the apical, non-bridging oxygens) in the $^2_\infty[Si_2O_5^{2-}]$ primitive cell. Third, the interactions fall in four broad groupings. Si(3*s*)–O(2*s*) bonding interactions are prominent in two of the bonding states at the bottom of the "O(2*s*)" band ($1a_1$ and $1b_2$ of Figures 4a and 4b). Si(3*p*)–O(2*s*) interactions are found at the top of the "O(2*s*)" band ($1e_2$ and $2a_1$ of Figures 4c and 4d), while the Si(3*p*)–O(2*p*) interactions are found at the bottom of the "O(2*p*)" band ($2b_2$ and $1e_1$ of Figures 4e and 4f). The non-bonding O(2*p*) states lie at the top of the "O(2*p*)" band, degeneracies removed by next-nearest-neighbor interactions.

Band Structure and Density of States of the Isolated $^2_\infty[Si_2O_5^{2-}]$ Framework and the Effect of Distortions

I. Band Structure for the p6mm Frame

The symmetry points and symmetry lines of first Brillouin zones of layer groups *p6mm*, *p31m*, *c1m1* and *c2/m* appear in Table 1. Because symmetry points $\mathbf{k}_\Gamma$ and $\mathbf{k}_K$ have the highest symmetry we will only present the band structure for these **k**-points and the wave vectors connecting them. The orbitals at $\mathbf{k}_\Gamma$ for the lower six bands of the *p6mm* sheet (see Fig. 5) are essentially the same as those appearing in Figure 4. The remaining eight bands are essentially non-bonding O(2*p*) combinations.

The dispersion of a band, i.e. the band width, is proportional to the magnitude of the interaction integral H_{ij} (cf. Ashcroft and Mermin 1976 or Albright, Burdett and Whangbo 1985 for a discussion of the tight-binding method). The bands with the greatest dispersion (Fig. 5) involve the interaction of Si(3*s*) and O(2*s*) orbitals, while the flat bands at −33 eV arise from Si(3*p*)–O(2*s*) interactions. We will see later that the states at −33 eV make an important contribution to the bonding interaction (cf. Fig. 7 below and the discussion of crystal-orbital-overlap populations), their large number compensating for the weak Si(3*p*)–O(2*s*) interactions. Since the VIOP for O(2*s*) was taken to be −32.3 eV in these calculations, all states in the "O(2*s*)" bands have been stabilized through bonding and cannot be considered non-bonding.

In the "O(2*p*)" group of bands (those lying between −14 eV and −18 eV, Fig. 5), the bands with the greatest dispersion arise from Si(3*s*, 3*p*)–O(2*p*) interactions. Above these are the bands due to Si(3*p*)–O(2*p*) mixing with the non-bonded O(2*p*) bands lying at the top of the "O(2*p*)" bands. Some of the non-bonded O(2*p*) states are slightly destabilized relative to −14.8 eV, the VIOP for O(2*p*), by weak anti-bonding interactions. Discussions of the role of O(2*p*)–O(2*p*) interactions in causing dispersion in the non-bonded states can be found elsewhere (Fisher et al. 1977; Hughbanks 1985; Chadi et al. 1978).

II. Density of States

The density of states, DOS(E), is defined such that DOS(E)dE is the number of states in the interval E to E+dE. Since we are expressing our "crystal" orbitals as a *linear combination of atomic orbitals* (LCAO) we can "project out" specific atomic orbitals or linear combinations of atomic orbitals, it the manner of Ciraci and Batra (1977). The projected DOS of the apical, non-bridging and basal, bridging oxygens for the *p6mm* $^2_\infty[Si_2O_5^{2-}]$-frame appear in

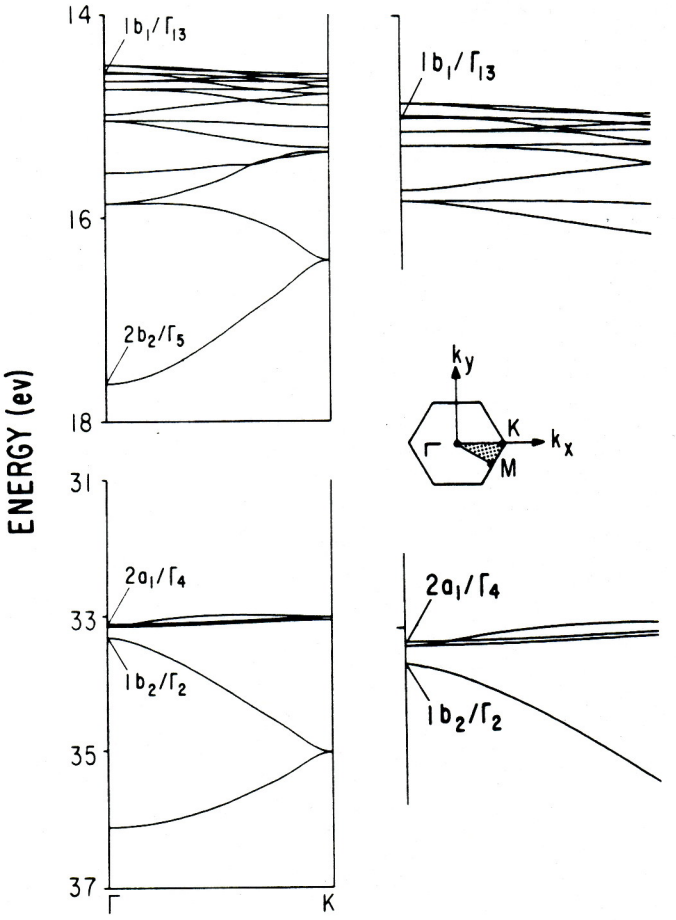

Fig. 5. Band structure of a *p6mm* tetrahedral sheet, $^{2}_{\infty}[Si_2O_5^{2-}]$, showing the first Brillouin zone with irreducible wedge (shaded), symmetry points and lines

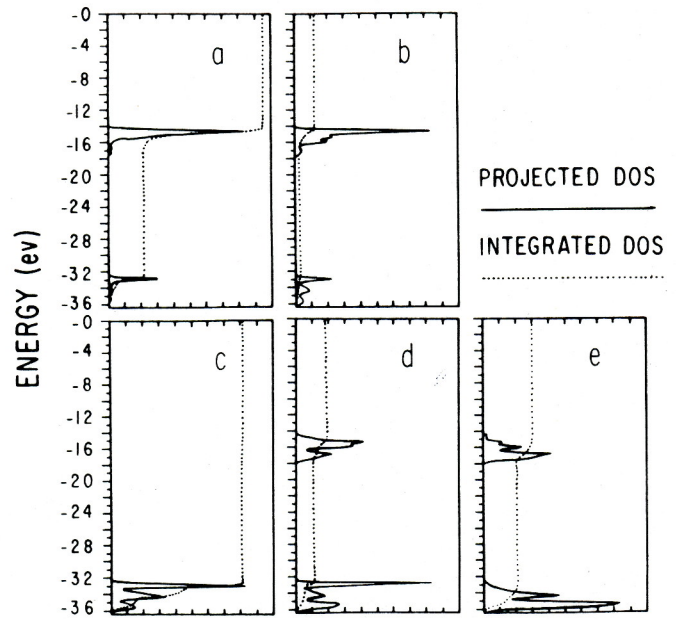

Fig. 6a–e. Density of states for selected atoms and orbitals of a *p6mm* tetrahedral sheet, $^{2}_{\infty}[Si_2O_5^{2-}]$,: (**a**) O_{apical}, (**b**) O_{basal}, (**c**) O_{basal} (2*s*), (**d**) Si, and (**e**) Si(3*s*)

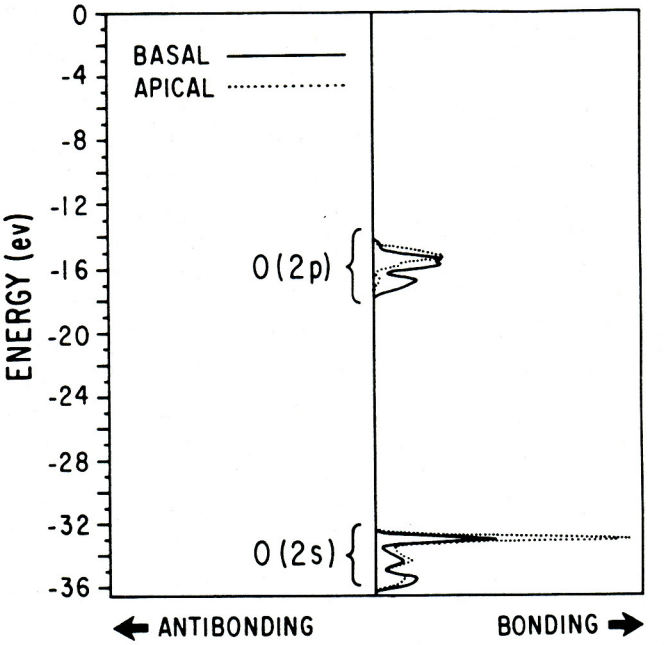

Fig. 7. Crystal orbital overlap population curves for $Si-O_{basal}$ (solid line) and $Si-O_{apical}$ (dashed line) bonds of a *p6mm* tetrahedral sheet, $^{2}_{\infty}[Si_2O_5^{2-}]$

Figures 6a and 6b, the projected DOS for the basal O(2*s*) atomic orbitals (AO's) in Figure 6c, and the projected DOS for the Si(3*s*) and Si(3*s*)+Si(3*p*) atomic orbitals are shown in Figures 6d and 6e. All projections are on an expanded scale.

The upper portion of the "O(2*p*)" bands, centered at about −15 eV, consists of non-bonded oxygen states. It is easy to see that the proportion of these non-bonded states is significantly higher for the apical than the basal oxygens. A comparison of the COOP curves (discussed below) and the projected DOS for both apical and basal oxygens confirms the non-bonded character of this peak. The extent of "sp-mixing" of the oxygen states (illustrated in Fig. 6c) is negligible, confirming our choice to disregard it in our qualitative discussion of bonding. It does occur to a noticeable extent for silicon orbitals and, as we would expect, the ratio of Si(3*s*) to Si(3*p*) decreases as the energy increases within either the "O(2*p*)" or, to a lesser extent, the "O(2*s*)" bands. The states centered at −33 eV at the top of the "O(2*s*)" bands (Figs. 6a, 6b and 6e) are exclusively Si(3*p*)−O(2*s*) σ-bonding (cf. Breeze and Perkins 1973). The projected DOS appear to confirm the broad outlines presented in the simple orbital analysis based on symmetry and perturbation theory.

III. Crystal Orbital Overlap Populations

When all bonds of a given type, Si−O bonds in this case, are set to equal length the overlap population, $n(Si-O)$, ranks the bonds according to their relative length, indicating which bonds should be longer or shorter in an actual structure. The overlap population for the apical Si−O bond is 0.54 and 0.50 for the basal bond in a *p6mm* frame where all bond lengths are set at 1.618Å. Based on these overlap populations we would expect the apical bond should be shorter than the basal.

The COOP curve for the two Si−O bonds (Fig. 7) shows that orbital interactions of O(2*s*) with Si(3*s*) and

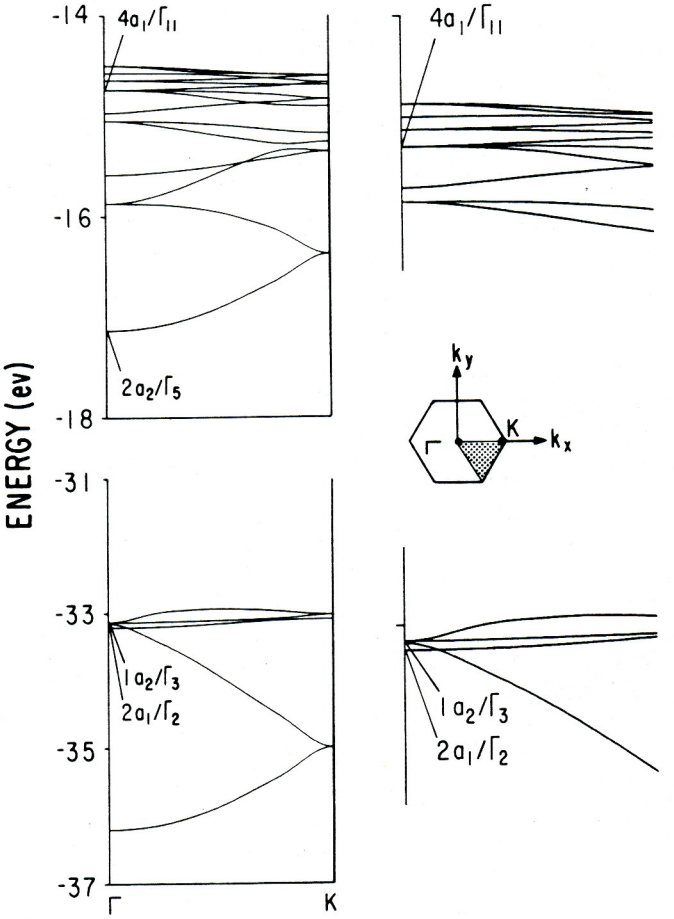

Fig. 8. Band structure of a *p31m* tetrahedral sheet, $^{2}_{\infty}[Si_2O_5^{2-}]$, showing the first Brillouin zone with irreducible wedge (shaded), symmetry points and lines

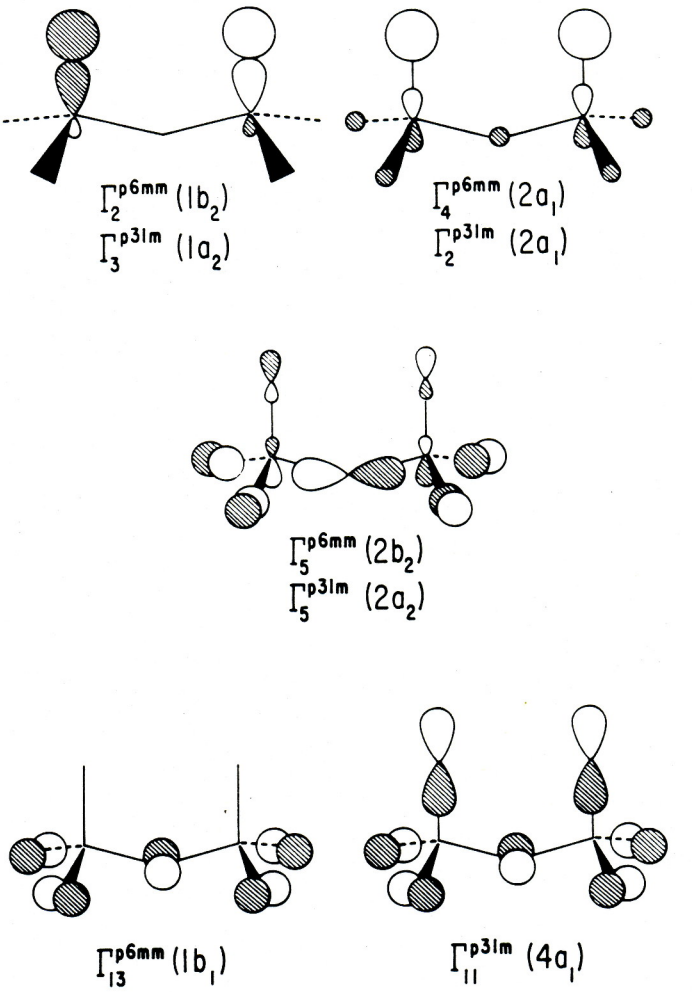

Fig. 9. Selected states of *p6mm* and *p31m* $^{2}_{\infty}[Si_2O_5^{2-}]$ tetrahedral sheets at the center of the Brillouin zone

Si(3*p*) account for about half of the bonding overlap population in those bonds. The COOP curve weights the number of states within a given energy interval by the overlap population for a specific bond. It follows that an interval with many states characterized by modest overlap can be as important as an energy interval encompassing for fewer states but with considerably greater overlap (cf. Breeze and Perkins (1973) and their discussion of DOS and orbital coefficients).

The former case is illustrated by the peak centered at −33 eV arising from Si(3*p*)−O(2*s*) interactions (cf. Figs. 6e and 7), while the latter by Si(3*s*)−O(2*s*) interactions in the range −34 to −36 eV. Although there are three times as many bonding interactions involving O(2*p*) orbitals than O(2*s*) in the frame, their overlap with Si is less. Hence, O(2*s*) orbitals compensate for fewer number of states, and a less favorable energy match, by a much greater overlap.

Distortion of the Isolated Frame by Tetrahedral Rotation and Tilting

Rotation and tilting of the silicate tetrahedra induce only minor changes in the $^{2}_{\infty}[Si_2O_5^{2-}]$ frame; the band structure for *p31m* appears in Figure 8. The states stabilized or destabilized (in no case was the energy change more than 0.5 eV) appear to be influenced more often by next-nearest-neighbor, oxygen-oxygen interactions than direct, nearest-neighbor interactions. This is best illustrated by the four states at the center of the Brillouin zone (Fig. 9) most influenced by the tetrahedral rotations which lower the symmetry from *p6mm* to *p31m*: $\Gamma_2^{p6mm}(1b_2) \rightarrow \Gamma_3^{p31m}(1a_2)$, $\Gamma_4^{p6mm}(2a_1) \rightarrow \Gamma_2^{p31m}(2a_1)$, $\Gamma_5^{p6mm}(2b_2) \rightarrow \Gamma_5^{p31m}(2a_2)$, $\Gamma_{13}^{p6mm}(1b_1) \rightarrow \Gamma_{11}^{p31m}(4a_1)$. The symbol "$\Gamma_n^{p6mm}$" indicates the n^{th} band of layer group *p6mm* at $\mathbf{k} = \mathbf{k}_\Gamma$, while the symbol in brackets uses the notation common in molecular orbital theory to specify the irreducible representation of a given combination of orbitals.

The case of $\Gamma_{13}^{p6mm}(1b_1) \rightarrow \Gamma_{11}^{p31m}(4a_1)$ is quite interesting. In *p6mm* there is no combination of apical oxygen orbitals transforming as b_1. Thus, $\Gamma_{13}^{p6mm}(1\ b_1)$ is a strictly non-bonding combination of $O_{basal}(2p_x, 2p_y)$ orbitals. Combinations of orbitals that transformed as "b_1" transform as "a_1" as a result of the tetrahedral-rotation distortion lowering the layer-group symmetry from *p6mm* to *p31m*. There are now combinations of both $O_{apical}(2p_z)$ and $O_{basal}(2p_x, 2p_y)$ orbitals transforming as a_1 and mixing occurs. Still, it is the next-nearest-neighbor interactions which stabilize $\Gamma_{11}^{p31m}(4a_1)$ relative to $\Gamma_{13}^{p6mm}(1b_1)$.

If the result of the distortion were to follow the

analysis given by Tossell (1984), states such as $\Gamma_2^{p6mm}(1b_2) \rightarrow \Gamma_3^{p31m}(1a_2)$, $\Gamma_4^{p6mm}(2a_1) \rightarrow \Gamma_2^{p31m}(2a_1)$, and $\Gamma_{13}^{p6mm}(1b_1) \rightarrow \Gamma_{11}^{p31m}(4a_1)$ would not be expected to change in energy. Of all the states, the energy of $\Gamma_5^{p6mm}(2b_2) \rightarrow \Gamma_5^{p31m}(2a_2)$ changes the most. The destabilization of this state is consistent with what we would predict based on nearest-neighbor interactions. Still, the observed destabilization can also be easily rationalized if we look at next-nearest-neighbor, oxygen-oxygen interactions. We will not discuss the *p31m* → *c1m1* tilting distortion since the effect on orbital interactions is negligible beyond the lifting of degeneracies at $\mathbf{k}_\Gamma$ and $\mathbf{k}_K$.

Electronic Structure and Bonding in Kaolinite, Lizardite, Pyrophyllite and Talc: Perturbation of the $^2_\infty[Si_2O_5^{2-}]$ Frame

I. Orbital interactions in Lizardite (p31m) and Talc (c2/m)

The bands from the isolated, *p6mm* $^2_\infty[Si_2O_5^{2-}]$-frame (Fig. 5) can be readily traced in the band structure diagram for lizardite *p31m* (Fig. 10), the added bands arise from O(2*s*, 2*p*)−H(1*s*) interactions in the hydroxyls of the mineral and the non-bonding states associated with these extra oxygens. We would anticipate little if any orbital interaction between magnesium orbitals and states in the "O(2*s*)" bands. Lizardite states: $\Gamma_5(1a_2)$, $\Gamma_7(4a_1)$ and $\Gamma_8(2a_2)$ are quite similar in appearance and energy to the *p6mm*-frame states: $\Gamma_2^{p6mm}(1b_2)$, $\Gamma_4^{p6mm}(2a_1)$, and $\Gamma_5^{p6mm}(2b_2)$.

Orbital interactions between magnesium atoms and the frame are rather weak and appear to be limited to $\Gamma_{14}(3a_2)$, derived from the *p6mm*-state $\Gamma_9^{p6mm}(3b_2)$. $\Gamma_9^{p6mm}(3b_2)$, a non-bonding state in *p6mm*, has the properties necessary for interactions with magnesium; i.e., it is among the topmost filled states with prominent apical orbitals directed toward the octahedral site. The importance of orbitals directed toward the octahedral site can be seen in the projected DOS for apical O($2p_z$) and [O($2p_x$)+O($2p_y$)], appearing in Figures 11a and 11b. The peak in the projected DOS of O($2p_z$) at about −15.5 eV below the non-bonded O(2*p*) states, and absent in the DOS curve for the in-plane [O($2p_x$)−O($2p_y$)] combination, arises from the interaction with magnesium.

The relation between talc and lizardite is straightforward. All "$^2_\infty[Si_2O_5^{2-}]$-frame" bands are doubled and there are only half as many "hydroxyl" bands. Other than this there is no major difference between talc and lizardite.

II. Orbital Interactions in Kaolinite (c1m1) and Pyrophyllite (c2/m)

Kaolinite and pyrophyllite differ significantly from the magnesium-containing minerals discussed above. Unlike magnesium, aluminum (even in octahedral coordination and with Al−O bond lengths significantly longer than the Si−O bond) behaves like silicon in many respects. The projected density of states for Al(3*s*), Si(3*s*), Al and Si are shown (on an expanded scale) in Figure 12 and the COOP curves for Al−O and Si−O bonds in Figure 13. The similarity is quite striking, from the nearly equal involvement of O(2*s*) and O(2*p*) interactions in their bond with oxygen to the structure of their DOS profiles.

Our primary concern is the perturbation of the electronic structure of the $^2_\infty[Si_2O_5^{2-}]$ frame through its interactions with aluminum. The projected-DOS diagrams for $O_{apical}(2p_z)$ (on an expanded scale) and the in-plane, $[O_{apical}(2p_x)+O_{apical}(2p_y)]$ combination appear in Figure 14, illustrating the prominence of O($2p_z$) in the interac-

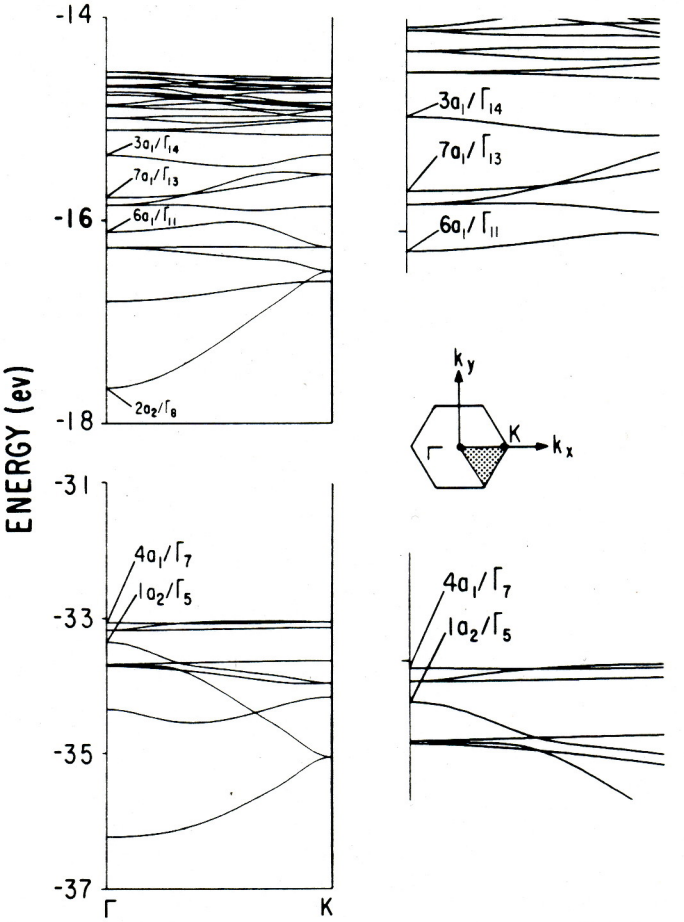

Fig. 10. Band structure of an *idealized*, single-layer lizardite ($^2_\infty[Mg_3(OH)_4Si_2O_5]$, layer-group: *p31m*) showing the first Brillouin zone with irreducible wedge (shaded), symmetry points and lines

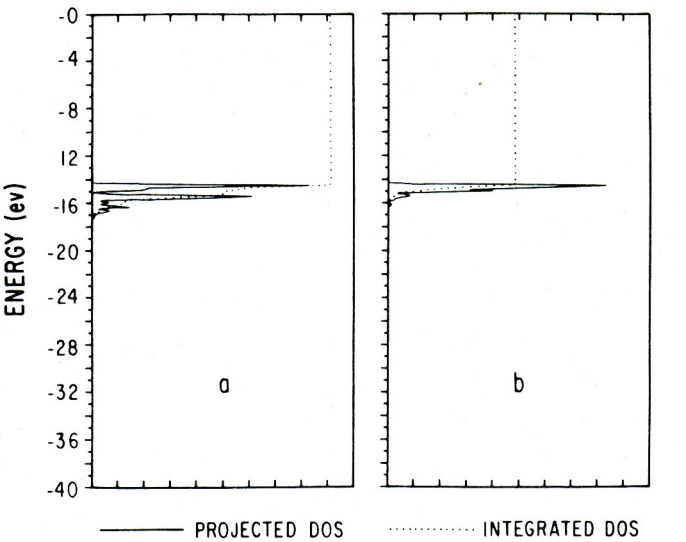

Fig. 11a, b. Density of states for apical-oxygen, O(2*p*) orbitals of an *idealized*, single-layer lizardite ($^2_\infty[Mg_3(OH)_4Si_2O_5]$, layer-group: *p31m*): (**a**) $O_{apical}(2p_z)$, (**b**) $O_{apical}(2p_x+2p_y)$

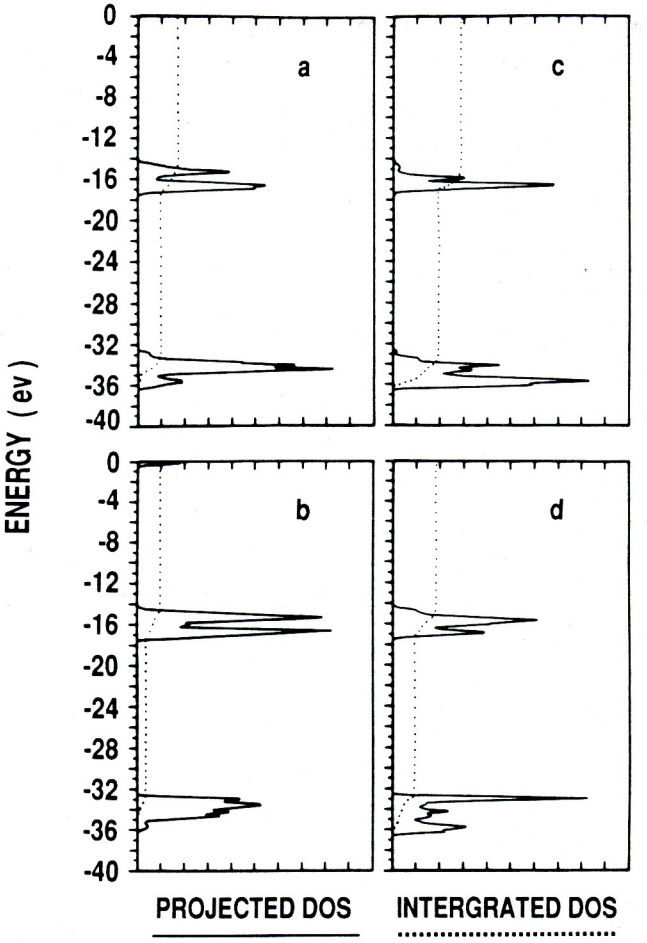

Fig. 12a–d. Density of states for: (**a**) Al(3*s*), (**b**) Si(3*s*), (**c**) Al and (**d**) Si of an *idealized*, single-layer kaolinite ($^2_\infty[Al_2(OH)_4Si_2O_5]$, layer-group: *c1m1*)

tions of the frame with aluminum. The projected-DOS curves direct our attention to bands in the vicinity of -15.5 eV and -17 eV in the "O(2*p*)" bands. The COOP curves (Fig. 13b), on the other hand, suggest Al–O orbital interactions involving the "O(2*s*)" band.

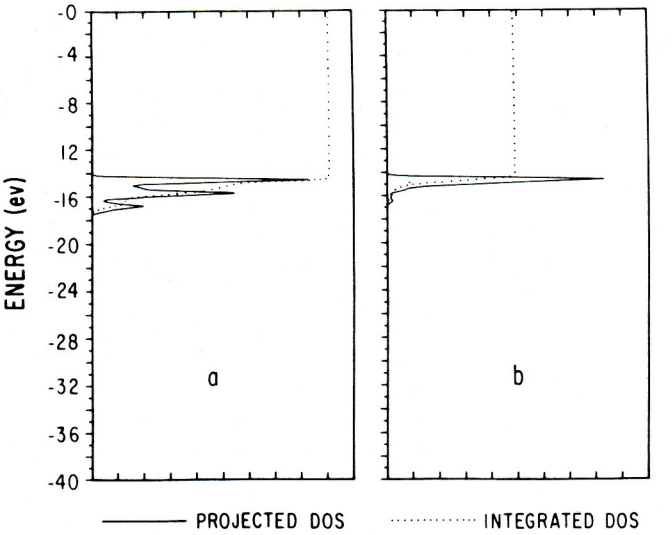

Fig. 14a, b. Density of states for apical-oxygen, O(2*p*) orbitals of an *idealized*, single-layer kaolinite ($\infty[Al_2(OH)_4Si_2O_5]$, layer-group: *c1m1*):] (**a**) O_{apical} ($2p_z$), (**b**) O_{apical} ($2p_x+2p_y$)

The band structure for kaolinite *c1m1* appears in Figure 15. The $^2_\infty[Si_2O_5^{2-}]$ frame in this idealized structure for our hypothetical, idealized, *c1m1* kaolinite is the same as that used in the *p31m* isolated $^2_\infty[Si_2O_5^{2-}]$ frame (Fig. 2b). The reduction of symmetry from *p31m* to *c1m1* lifts two-fold degeneracies at $\mathbf{k}_\Gamma$ and $\mathbf{k}_K$ but, in and of itself, has little effect on the band structure. The differences between the band structure of the isolated, *p31m* frame and that of kaolinite *c1m1* (aside from the additional "hydroxyl" bands) are due mainly to perturbations of the frame by aluminum.

The electronic structure of pyrophyllite is basically the same as kaolinite. As in the case of talc, there is a doubling of $^2_\infty[Si_2O_5^{2-}]$-frame bands and the absence of half of the "hydroxyl" bands but no other qualitative differences.

Atomic and Overlap Populations in Phyllosilicate Minerals

In Table 2 we list the overlap populations for $Si-O_{apical}$ and $Si-O_{basal}$ bonds averaged over the first Brillouin zone

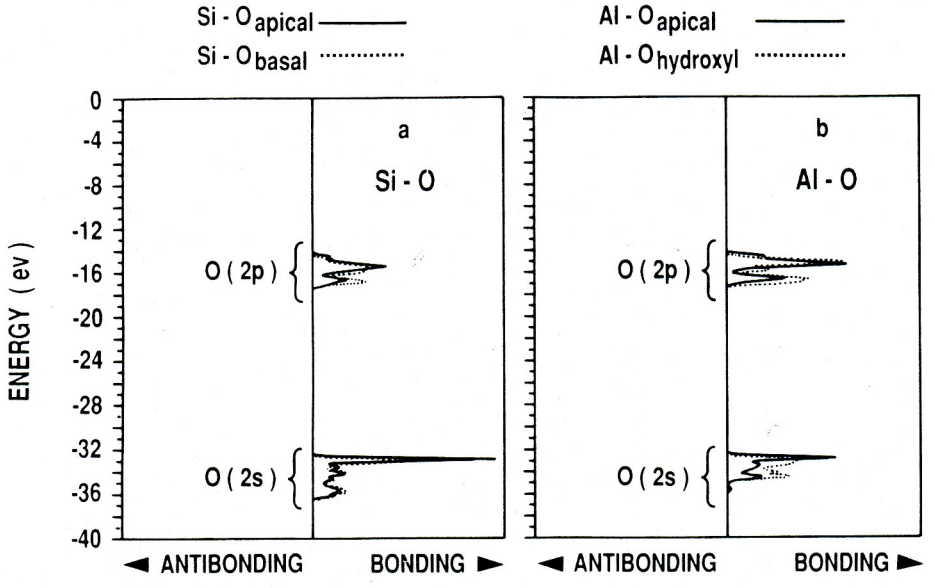

Fig. 13a, b. Crystal orbital overlap population curves for: (**a**) Si–O bonds (basal and apical) and (**b**) Al–O bonds (apical and hydroxyl) of an *idealized*, single-layer kaolinite ($^2_\infty[Al_2(OH)_4Si_2O_5]$, layer-group: *c1m1*)

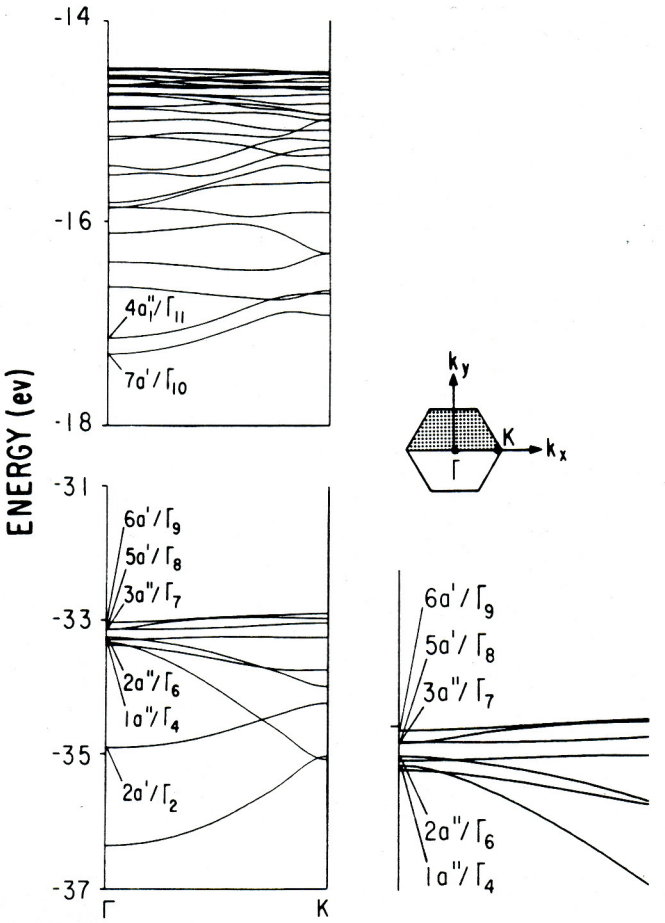

Fig. 15. Band structure of an *idealized*, single-layer kaolinite ($^2_\infty[Al_2(OH)_4Si_2O_5]$, layer-group: *c1m1*) showing the first Brillouin zone with irreducible wedge (shaded), symmetry points and lines

for the *p6mm* and *p31m* $^2_\infty[Si_2O_5^{2-}]$ frames and the idealized structures for kaolinite, lizardite, pyrophyllite and talc. From these results we would predict that $d(Si-O_{apical}) < d(Si-O_{basal})$ in all of these minerals. The differences, however, between $n(Si-O_{apical})$ and $n(Si-O_{basal})$ for the minerals are significantly less than in the isolated frames and about the same for all the minerals.

The estimated charges of the ions, from atomic populations, are also found in Table 2. The charges on Si and O_{basal} are essentially the same as for the isolated frames, but we can see that the charge on O_{apical} has decreased significantly from -1.62 to about -1.39 (for the Al-containing minerals) and -1.46 (for the Mg-containing minerals). Atomic and overlap populations suggest that coordination of the apical oxygens in the mineral by the octahedral cations reduces the charge on the apical oxygen while having little effect on the $Si-O_{apical}$ bond strength.

The projected DOS of O_{apical} for lizardite and kaolinite appear in Figures 11 and 14. We can clearly see that these differ significantly from the projected DOS for O_{apical} in the isolated frames by having more states in the range -15 to -17 eV. These states have been stabilized primarily by orbital interactions between previously non-bonded, $O(2p_z)$ orbitals on the *apical* oxygen and the octahedral cations. The projected DOS for O_{apical} and O_{basal} are quite distinct, one from another, in the isolated $^2_\infty[Si_2O_5^{2-}]$-frames but appear to be similar in the minerals we are considering. The projected DOS for Si and O orbitals for lizardite and talc and for kaolinite and pyrophyllite are all essentially the same.

Conclusions

Distortions of the two-dimensional, infinite $^2_\infty[Si_2O_5^{2-}]$-frame through the rotation and tilting of the silicate tetrahedra lead to no major changes in the orbital interactions or the energetics we associate with orbital interactions. Both stabilization and destabilization of individual states occur with these distortions, traceable to next-nearest-neighbor oxygen-oxygen interactions.

Analysis of crystal-orbital-overlap-populations for the Si–O bond, projected DOS for Si(3*s*), Si(3*p*) and O(2*s*) as well as the band structure for the $^2_\infty[Si_2O_5^{2-}]$-frame demonstrate the importance of orbital interactions between Si(3*s*, 3*p*) and O(2*s*) atomic orbitals in bond formation. These interactions appear to account for about half of the bonding overlap in the Si–O bond.

In lizardite and talc there is little orbital interaction between the $^2_\infty[Si_2O_5^{2-}]$-frame and Mg(II). The valence-band structure for these minerals is essentially the superposition of *p6mm*-frame bands and bands arising structural hydroxyls. There is sufficient interaction between Mg(3*s*) and apical O(2*p*) orbitals to lower the $Si-O_{apical}$ overlap population and lead to the appearance of new bonding states in the apical–O(2*p*), projected-DOS diagram.

Orbital interactions between the $^2_\infty[Si_2O_5^{2-}]$-frame and Al(III) in kaolinite and pyrophyllite are important. The significance of next-nearest-neighbor, oxygen-oxygen interactions, in addition to direct $Al-O_{apical}$ interactions, is readily apparent. Direct, $Al-O_{apical}$ interactions involve primarily states that were non-bonding in the isolated frame.

It seems that we can view the electronic structure of phyllosilicates as simple perturbations of the electronic structure of the isolated $^2_\infty[Si_2O_5^{2-}]$-frame. Even in lizardite and talc, where the interaction is weakest, there are significant changes in the atomic population of the apical oxygens

Table 2. Crystal orbital overlap populations and ionic charges

Unit	$n(Si-O_{apical})$	$n(Si-O_{basal})$	$q(Si)$	$q(O_{apical})$	$q(O_{basal})$
$[Si_2O_5^{2-}]$, *p6mm*	0.54	0.50	2.47	−1.61	−1.24
$[Si_2O_5^{2-}]$, *p31m*	0.54	0.49	2.52	−1.62	−1.27
Lizardite	0.55	0.53	2.39	−1.46	−1.22
Talc	0.55	0.53	2.38	−1.46	−1.22
Kaolinite	0.52	0.51	2.49	−1.39	−1.25
Pyrophyllite	0.52	0.51	2.49	−1.39	−1.25

Table 3. Orbital parameters used in the extended Hückel calculations

Atom	Orbital	VOIP, eV	Exponent
Al	3*s*	−12.3	1.167
	3*p*	− 6.5	1.167
H	1*s*	−13.6	1.300
Mg	3*s*	− 9.0	0.950
	3*p*	− 4.5	0.950
O	2*s*	−32.3	2.275
	2*p*	−14.8	2.275
Si	3*s*	−17.3	1.383
	3*p*	− 9.2	1.383

and the overlap populations in the $Si-O_{apical}$ bond. The Si and O_{basal} atoms of the frame are as little affected by interactions of the frame with octahedral atoms as they are by rotational and tilting distortions of the frame.

Acknowledgements. R.H. is grateful to the National Science Foundation for its support of this work through Research Grant: CHE 8406119. W.B. is grateful the Cornell Chapter of Sigma Xi for its early support of this study under its Grants-in-Aid Program.

Appendix

The orbital parameters used in our extended Hückel, tight-binding calculations appear in Table 3. The important distances used in our calculations are: $d(Si-O)=1.618$ Å (Brindley and Brown 1980, p. 3), $d(Al-O)=1.924$ Å (mean $d(Al-O_{apical})$, Lee and Guggenheim 1981), $d(Mg-O)=2.067$ Å (mean $d(Mg-O)$, Mellini 1982), $d(O-H)=0.971$ Å ($d(H-O)$, Lee and Guggenheim 1981), $d(O-O)_{Mg,\ shared\text{-}edge}=2.430$ Å, and $d(O-O)_{Al,\ shared\text{-}edge}=2.567$ Å. The silicate tetrahedra have point symmetry $\bar{4}3m$ while coordination polyhedra for both magnesium and aluminum have point symmetry $\bar{3}m$. The octahedral sheet has layer group symmetry *p31m* in lizardite, *c1m1* in kaolinite, and *c2/m* in both talc and pyrophyllite. The $^2_\infty[Si_2O_5^{2-}]$, tetrahedral sheet has layer symmetry *p6mm* in lizardite and talc and *p31m* symmetry in kaolinite and pyrophyllite.

A set of 24 **k**-points for the *p6mm* layer group, 44 **k**-points for the *p31m* layer group, and 16 **k**-points for the *c1m1* and *c2/m* layer groups were used in the irreducible wedges of the first Brillouin zones (Cunningham 1974). Density of state and COOP calculations, which require integration over the first Brillouin zone, were based on these special **k**-point sets. We generated the **k**-point set for *p31m* by taking an irreducible wedge double that of *p6mm* and using symmetry to generate the extra points from the smaller *p6mm* set.

References

Albright T, Burdett JK, Whangbo M-H (1985) Orbital interactions in chemistry. John Wiley and Sons, New York

Aronowitz S, Coyne L, Lawless J, Rishpon J (1982) Quantum-chemical modeling of smectite clays. Inorg Chem 21:3589–3593

Ashcroft NW, Mermin N (1976) Solid state physics. Saunders College, Philadelphia, PA

Bennett AJ, Roth LM (1971) Electronic structure of defect centers in SiO_2. J Phys Chem Solids 32:1251–1261

Breeze A, Perkins PG (1973) Energy band structure of silica. J Chem Soc Faraday Trans II 69:1237–1242

Brindley GW, Brown G (1980) Crystal structures of clay minerals and their x-ray identification. Mineralogical Society, London

Brytov IA, Romashchenko YN, Shchegolev BF (1979) Electronic structure of the octahedral oxyanions of aluminum and silicon. Struct Chem (Engl Trans) 20:190–196

Chadi DJ, Laughlin RB, Joannopoulos JD (1978) Electronic structures of crystalline and amorphous SiO_2. In: Pantelides ST (ed) The physics of SiO_2 and its interfaces. Pergamon Press, New York, pp 55–59

Ciraci S, Batra IP (1977) Electronic-energy-structure calculations of silicon dioxide using the extended tight-binding method. Phys Rev B 15:4923–4934

Cunningham SL (1974) Special points in the two-dimensional Brillouin zone. Phys Rev B 10:4988–4994

Cusachs LC, Corrington JH (1970) Atomic orbitals from semi-empirical molecular orbital calculations. In: Sinanoglu O, Wiberg KB (eds) Sigma Molecular Orbital Theory. Yale University Press, New Haven, pp 256–272

Dikov YP, Debolsky EI, Romashenko YN, Dolin SP, Levin AA (1977) Molecular orbitals of $Si_2O_7^{6-}$, $Si_3O_{10}^{8-}$, etc., and mixed $(B, Al, P, Si)_m$ applied to clusters and x-ray spectroscopy data of silicates. Phys Chem Minerals 1:27–41

DiStefano TH, Eastman DE (1971) Photoemission measurements of the valence levels of amorphous SiO_2. Phys Rev Lett 27:1560–1562

Fisher B, Pollak RA, DiStefano TH, Grobman WD (1977) Electronic structure of SiO_2, $Si_xGe_{1-x}O_2$, and GeO_2 from photoemission spectroscopy. Phys Rev B 15:3193–3199

Gibbs GV, Hamil MM, Louisnathan SJ, Bartell LS, Yow H (1972) Correlations between Si−O bond length, Si−O−Si angle and bond overlap populations calculated using Extended Hückel molecular orbital theory. Am Mineral 57:1578–1613

Harrison WA (1980) Electronic structure and the properties of solids. W.H. Freeman and Co, San Francisco

Harrison WA (1977) The physics of solid state chemistry. Festkörperprobleme 17:135–155

Hoffmann R (1963) A extended Hückel theory. I. Hydrocarbons. J Chem Phys 39:1397–1412

Hoffmann R, Lipscomb WN (1962) Theory of polyhedral molecules. I. Physical factorizations of the secular equation. J Chem Phys 36:2179–2189

Hughbanks T (1985) Superdegenerate electronic energy levels in extended structures. J Am Chem Soc 107:6851–6859

Lee JH, Guggenheim S (1981) Single crystal x-ray refinement of pyrophyllite-1Tc. Am Mineral 66:350–357

Louisnathan SJ, Gibbs GV (1972a) The effect of tetrahedral angles on Si−O bond overlap populations for isolated tetrahedra. Am Mineral 57:1614–1642

Louisnathan SJ, Gibbs GV (1972b) Variation of Si−O distances in olivines, sodamelilite and sodium metasilicate as predicted by semi-empirical molecular orbital calculations. Am Mineral 57:1643–1663

Mellini M (1982) The crystal structure of lizardite 1T: hydrogen bonds and polytypism. Am Mineral 67:587–598

Pantelides ST, Harrison WA (1976) Electronic structure, spectra, and properties of 4:2-coordinated materials. I. Crystalline and amorphous SiO_2 and GeO_2. Phys Rev B 13:2667–2691

Pantelides ST (1977) Recent advances in the theory of electronic structure of SiO_2. Comments Solid State Phys 8:55–60

Peterson RC, Hill RJ, Gibbs GV (1979) A molecular-orbital study of distortions in the layer structures brucite, gibbsite and serpentine. Can Mineral 17:703–711

Schlüter M, Chelikowsky JR (1977) Electronic states in α-quartz (SiO_2). Solid State Commun 21:381–384

Schneider PM, Fowler WB (1976) Band structure and optical properties of silicon dioxide. Phys Rev Lett 36:425–428

Suitch PR, Young RA (1983) Atom positions in highly ordered kaolinite. Clays Clay Miner 5:357–366

Summerville RH, Hoffmann R (1976) Tetrahedral and other M_2L_6 transition metal dimers. J Am Chem Soc 98:7240–7254

Tinkham M (1964) Group Theory and Quantum Mechanics. McGraw-Hill, New York

Tossell JA (1984) A qualitative MO model for bridging bond angle variations in minerals. Phys Chem Minerals 11:81–84

Tossell JA (1975) The electronic structures of silicon, aluminum, and magnesium in tetrahedral coordination with oxygen from SCF-Xα MO calculations. J Am Chem Soc 97:4840–4844

Tossell JA, Gibbs GV (1977) Molecular orbital studies of geometries and spectra of minerals and inorganic compounds. Phys Chem Minerals 2:21–57

Tossell JA, Vaughan DJ, Johnson KH (1973) X-ray photoelectron, x-ray emission and UV spectra of SiO_2 calculated by the SCF-Xα scattered wave method. Chem Phys Lett 20:329–334

Vainshtein BK (1981) Modern Crystallography. I. Symmetry of crystals, Springer-Verlag, New York

Whangbo M-H, Hoffmann R, Woodward RB (1979) Conjugated one and two dimensional polymers. Proc R Soc London Ser A 366:23–46

Zvyagin BB (1960) Electron-diffraction determination of the structure of kaolinite. Soviet Phys Crystallogr (Engl Trans) 5:32–42

Received July 10, 1987